JACS Au
AN OPEN ACCESS JOURNAL OF THE AMERICAN CHEMICAL SOCIETY

pubs.acs.org/jacsau
Article

Leveraging Concentration Imbalance-Driven DNA Circuit as an Operational Amplifier to Enhance the Sensitivity of Hepatitis B Virus DNA Detection with Hybridization-Responsive DNA-Templated Silver Nanoclusters

Suo Lv,[#] Qunyan Yao,[#] Jiasheng Yi, Jingyi Si, Yifan Gao, Shao Su,* and Changfeng Zhu*

Cite This: *JACS Au* 2024, 4, 2323−2334

ABSTRACT: Hepatitis B virus (HBV) infection remains a major global health concern, necessitating the development of sensitive and reliable diagnostic methods. In this study, we propose a novel approach to enhance the sensitivity of HBV DNA detection by leveraging a concentration imbalance-driven DNA circuit (CIDDC) as an operational amplifier, coupled with a hybridization-responsive DNA-templated silver nanocluster (DNA-AgNCs) nanoprobe named Q·C6-AgNCs. The CIDDC system effectively converts and amplifies the input HBV DNA into an enriched generic single-stranded DNA output, which subsequently triggers the fluorescence of the DNA-AgNCs reporter upon hybridization, generating a measurable signal for detection. By incorporating the DNA circuit, we not only achieved enhanced sensitivity with a lower detection limit of 0.11 nM but also demonstrated high specificity with single-base mismatch discriminability for HBV DNA detection. Additionally, this mix-and-detect assay format is simple, user-friendly, and isothermal. This innovative strategy holds promise for advancing molecular diagnostics and facilitating the effective management of HBV-related diseases.

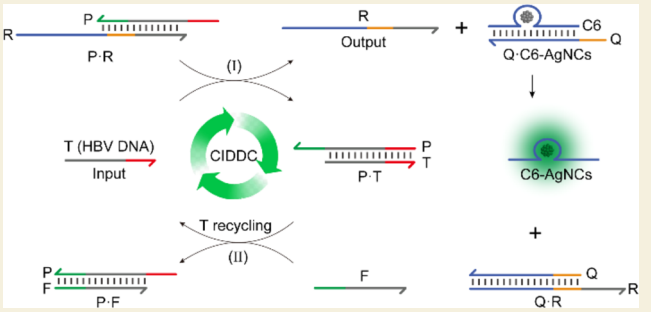

KEYWORDS: *DNA-templated silver nanocluster, hepatitis B virus, DNA circuit, fluorescent nanoprobe, biosensor*

INTRODUCTION

Despite the availability of safe and effective Hepatitis B virus (HBV) vaccines since the 1980s, HBV infection continues to pose a significant global public health challenge.[1,2] According to the latest statistics from the World Health Organization (WHO), an estimated 254 million people were living with chronic hepatitis B infection worldwide in 2022, resulting in 1.1 million deaths from hepatitis B-related end-stage liver diseases such as cirrhosis and hepatocellular carcinoma.[3,4] Although no definitive cure for HBV infection exists, early detection plays a crucial role by facilitating timely intervention and treatment, thereby reducing the risk of disease progression and transmission. Nucleic acid detection methods, notably polymerase chain reaction (PCR), are capable of identifying relatively low levels of viral genetic material in the bloodstream, offering the ability to detect HBV infection at an early stage even before the onset of symptoms or seroconversion.[5,6] In contrast, serological tests rely on the development of antibodies, which may require a longer duration to become detectable.[7]

PCR-based methods have historically been the prevailing approach for nucleic acid testing of viruses. However, their reliance on specialized thermal cyclers and sophisticated operators has hindered their use in highly endemic areas, which are usually developing regions. Consequently, there is a pressing need to develop cost-effective and user-friendly platforms for HBV detection. In this regard, fluorescent analytical methods have garnered significant interest due to their convenience, rapidity, and high sensitivity.[8,9] Nevertheless, the application of these methods is largely hampered by the inherently poor photostability of conventional organic fluorophores. In recent decades, fluorescent nanomaterials, such as quantum dots (QDs),[10] upconversion nanoparticles (UCNPs),[11] and noble metallic nanoclusters (NMNCs),[12−17] have emerged as highly appealing tools for a diverse range of applications in bioimaging, biosensing, and other fields where enhanced brightness, photostability, and spectral tunability are crucial. Among the various fluorescent nanomaterials, DNA-templated silver nanoclusters (DNA-AgNCs) have drawn

Received: April 1, 2024
Revised: May 17, 2024
Accepted: May 21, 2024
Published: May 31, 2024

https://doi.org/10.1021/jacsau.4c00291
JACS Au 2024, 4, 2323−2334

Scheme 1. Design Strategy for the DNA-AgNCs Probe and Principle of HBV DNA Detection[a]

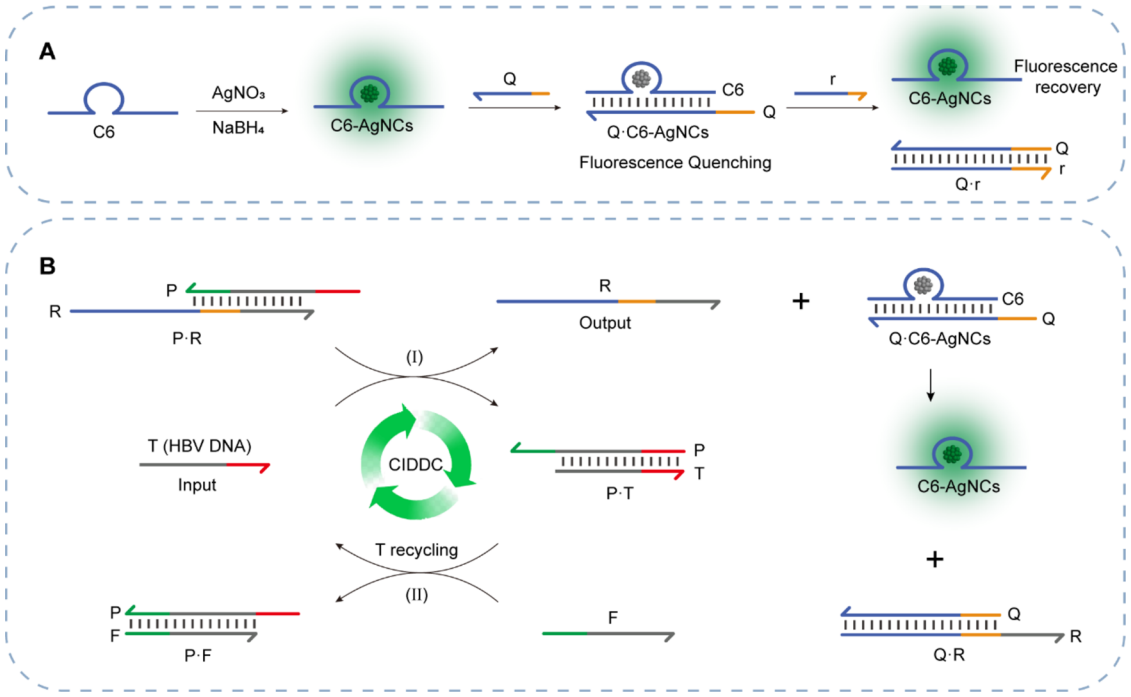

[a](A) Schematic illustration depicting the design of DNA-AgNCs nanoprobe. (B) Schematic illustration demonstrating the operational mechanism of the CIDDC and the sensing principle of the CIDDC-empowered assay for HBV DNA.

especially significant attention due to their exceptional characteristics. The crystal structures and corresponding optical properties of DNA-AgNCs are highly template sequence-dependent.[18,19] In addition, DNA-AgNCs exhibit remarkable environmental sensitivity, with their photophysical properties modulated by alterations in the sequence or structure of the DNA templates.[20] Notably, the structures of DNA templates can be precisely and programmably regulated through specific biological processes, such as hybridization, unfolding, and enzymatic digestion, which significantly enhance the versatility and potential biomedical applications of DNA-AgNCs.[21,22] For instance, we found that the specific hybridization between the target viral DNAs and the stem-loop probes resulted in the opening of the closed stem-loop structures, sequentially exposing DNA sequences that served as templates for the *in situ* synthesis of AgNCs.[23] In a separate study, we demonstrated that hybridization of the target viral DNA with two probe segments forms a unique ternary DNA structure featuring a cytosine-rich loop, serving as a template for the AgNC synthesis.[24] Leveraging these advantageous qualities, DNA-AgNCs have found extensive utility in detecting ions, small molecules, nucleic acids, and protein biomarkers.[25−31]

DNA-AgNC-based sensors, while offering unique advantages, do have inherent limitations in terms of sensitivity. To address this challenge and enhance detection sensitivity, the incorporation of signal amplification strategies is often necessary. Enzyme-free signal amplification proves to be more advantageous in the design of AgNC-based sensors due to the strong interference of sulfide or chloride ions commonly found in enzyme storage solutions or reaction buffers, which can negatively impact the formation and fluorescence signal of AgNCs. Furthermore, enzyme-free signal amplification strategies offer the benefits of assay simplicity, cost-effectiveness, and ease of optimization compared to enzyme-assisted signal amplification methods. Toehold-mediated strand displacement (TMSD) has received extensive attention and research in the field of enzyme-free isothermal amplification.[32] A series of methods, such as hybrid chain reaction (HCR),[33−35] catalytic hairpin assembly (CHA),[36−38] and entropy-driven catalysis (EDC),[39,40] have been employed in this context and have proven successful in detecting a wide variety of targets. Recently, Fan et al. explored an innovative enzyme-free amplification circuit with high efficiency by strategically manipulating the relative concentrations of reactants to prompt rapid displacement of DNA strands.[41] This groundbreaking DNA integrated circuit (DIC) system boasts a versatile architecture constructed from the integration of large-scale DNA-based programmable gate arrays (DPGAs). Interconnected via generic single-stranded oligos acting as a uniform transmission signal (DNA-UTS), the communication within this DIC system is orchestrated by recruiting concentration-anomalyzed DNA circuits (CIDDCs) as adaptors. These adaptors harness the concentration disparity between a high-concentration fuel strand and a low-concentration input strand (specifically, the output strand from an upstream gate) to drive a cyclic TMSD reaction, yielding a robust signal output (i.e., the input strand to a downstream gate). One of the key attributes of these adaptors is their exceptional capability to transmit DNA-UTS between gates and DPGAs with minimal signal attenuation. This quality plays a pivotal role in enabling the construction of large-scale DPGA networks with optimal performance. When applied in sensing applications, CIDDCs exhibit potent signal amplification capabilities. The CIDDC amplifiers efficiently amplify and convert the input signal, that is, the target strand, into output DNA-UTS, thereby enhancing sensitivity in the detection of target input strand. Inspired by these findings, we herein introduce a highly sensitive

https://doi.org/10.1021/jacsau.4c00291
JACS Au 2024, 4, 2323−2334

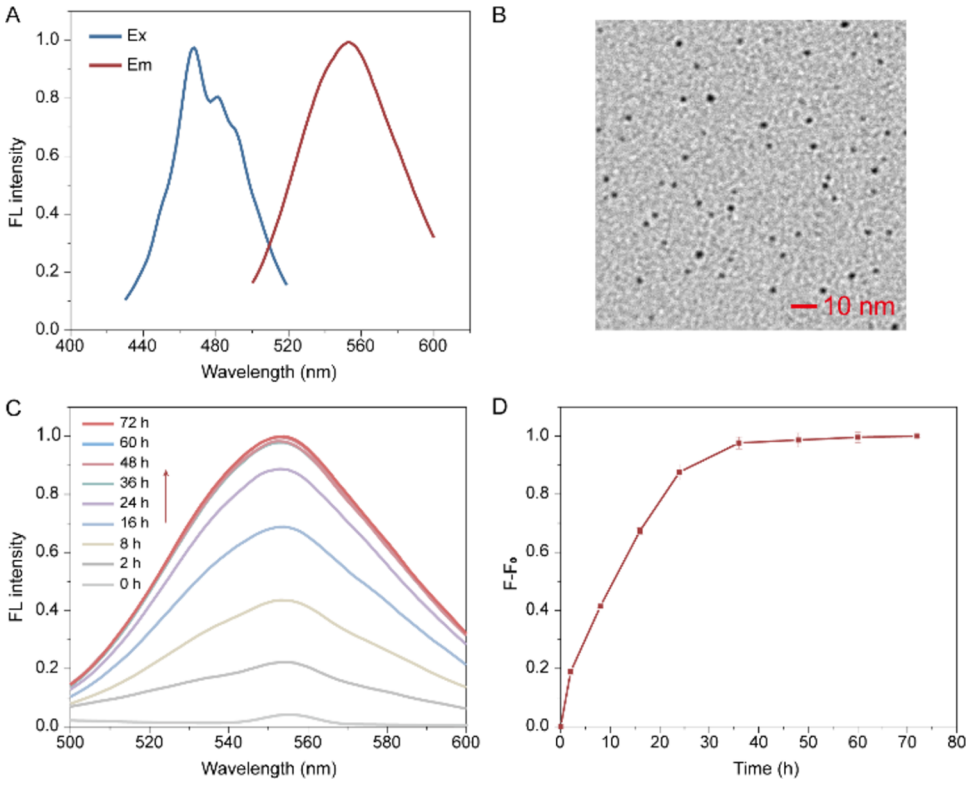

Figure 1. Synthesis and characterization of C6-AgNCs. (A) Fluorescence excitation (Ex) and emission (Em) spectra of C6-AgNCs. (B) TEM image showcasing the morphology of C6-AgNCs. (C) Fluorescence spectra of C6-AgNCs at different reduction times after the addition of $NaBH_4$. (D) Temporal fluorescence changes of C6-AgNCs upon varying the duration of $NaBH_4$ reduction.

fluorescent sensing platform for HBV DNA detection. Leveraging the fluorescent intensity of hybridization-responsive DNA-AgNCs as the out signal, coupled with a CIDDC serving as the signal amplifier, we successfully achieve both qualitative and quantitative detection of the virus by monitoring fluorescence changes in DNA-AgNCs before and after the introduction of HBV DNA.

RESULTS AND DISCUSSION

Design of the DNA-AgNCs Probe and Principle of the Assay

As depicted in Scheme 1A, the initial AgNC probe, denoted as C6-AgNCs, comprises a synthetic single-stranded DNA oligo (C6 strand) containing six consecutive cytosine bases (C6 domain). The strong affinity of the cytosine-rich domain with silver ions enables it to serve as a nucleation site for AgNC formation. *In situ* reduction of silver ions within the C6 domain is achieved using sodium borohydride ($NaBH_4$), resulting in a yield of green-emitting AgNCs. Upon the hybridization of C6 strand with the Q strand, a partial double-stranded Q·C6 structure is formed, featuring a C6 loop on the C6 strand and a toehold (orange region) at the 5′ end of the Q strand. This conformational change in the DNA template leads to fluorescence quenching of AgNCs (Q·C6-AgNCs). However, once introducing the r strand, which is complementary to the Q strand, it triggers the TMSD reaction, causing the dissociation of the Q strand from C6-AgNCs and thereby recovering the fluorescence of C6-AgNCs.

To create a fluorescent sensing platform for HBV DNA, we have designed a DNA-AgNCs-based system that incorporates a CIDDC as a signal amplifier. As illustrated in Scheme 1B, the sensing principle of this platform relies on the amplification effect of CIDDC, which converts the presence of the target strand, i.e., HBV DNA, into a substantial output of R strands. The R strand contains the complete sequence of r strand along with a few additional bases at the 3′ end (gray region). This process ultimately leads to the liberation and sequential fluorescence recovery of the C6-AgNCs. The CIDDC consists of two essential elements: a partial double-stranded P·R structure with a toehold (red region) at the 5′ end of the P strand and the Fuel (F) strand. It is important to note that the hybridization free energies of P·R, P·T, and P·F are essentially equal. Upon the introduction of HBV DNA (target, T strand), it binds to the toehold domain on the P strand, initiating branch migration and triggering a TMSD reaction (I). This TMSD generates the duplex strand P·T, featuring a toehold domain (green) at the 3′ end of the P strand while releasing the R strand. The F strand acts as an invader that selectively binds to the toehold region of P·T, inducing another TMSD reaction (II). This process ultimately leads to the displacement of the incumbent T strand to form a duplex strand P·F with a toehold region (red) at the 5′ end of the P strand, which facilitates a reverse TMSD reaction. However, due to the significantly higher concentration of the F strand compared to the T strand, a concentration-disequilibrium force drives the effective release of the T strand. The liberated T strand then binds to another P·R complex, initiating the next cycle of TMSD reactions and target strand recycling. Through the amplification effect, the initial introduction of a small quantity of T strand ultimately leads to a significant accumulation of free R strands as the output of this CIDDC. Such an abundant pool of R strands subsequently binds to the toehold region of the Q·C6-AgNCs complex, triggering the liberation and

https://doi.org/10.1021/jacsau.4c00291
JACS Au 2024, 4, 2323−2334

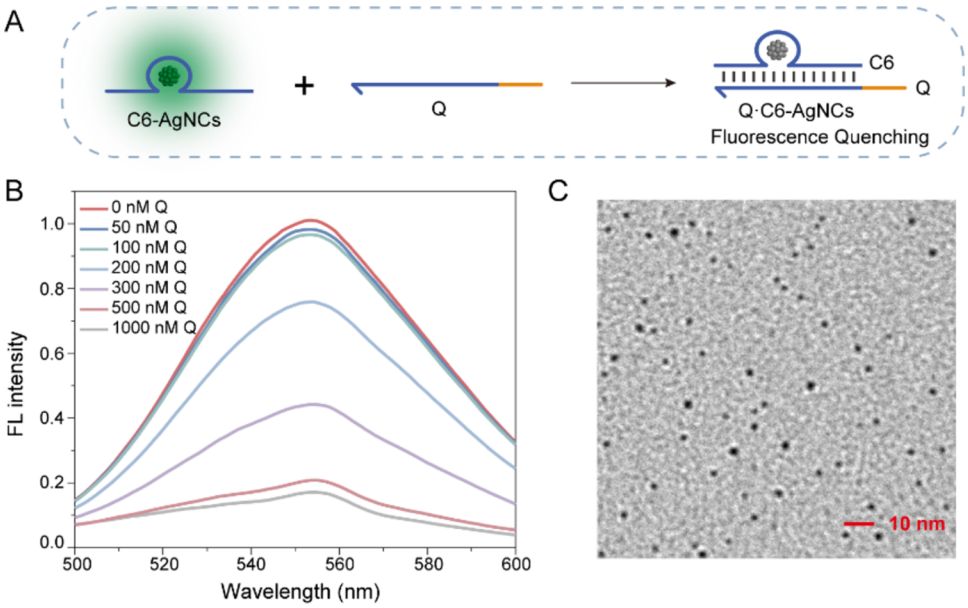

Figure 2. Fluorescence quenching of C6-AgNCs occurs upon hybridization with strand Q. (A) Schematic illustration demonstrating the fluorescence quenching of C6-AgNCs upon hybridization with the complementary strand, Q. (B) Fluorescence spectra of 300 nM C6-AgNCs in the presence of Q with varying concentrations (50, 100, 200, 300, 500, and 1000 nM). (C) TEM image displaying the morphology of C6-AgNCs quenched by the Q strand (500 nM).

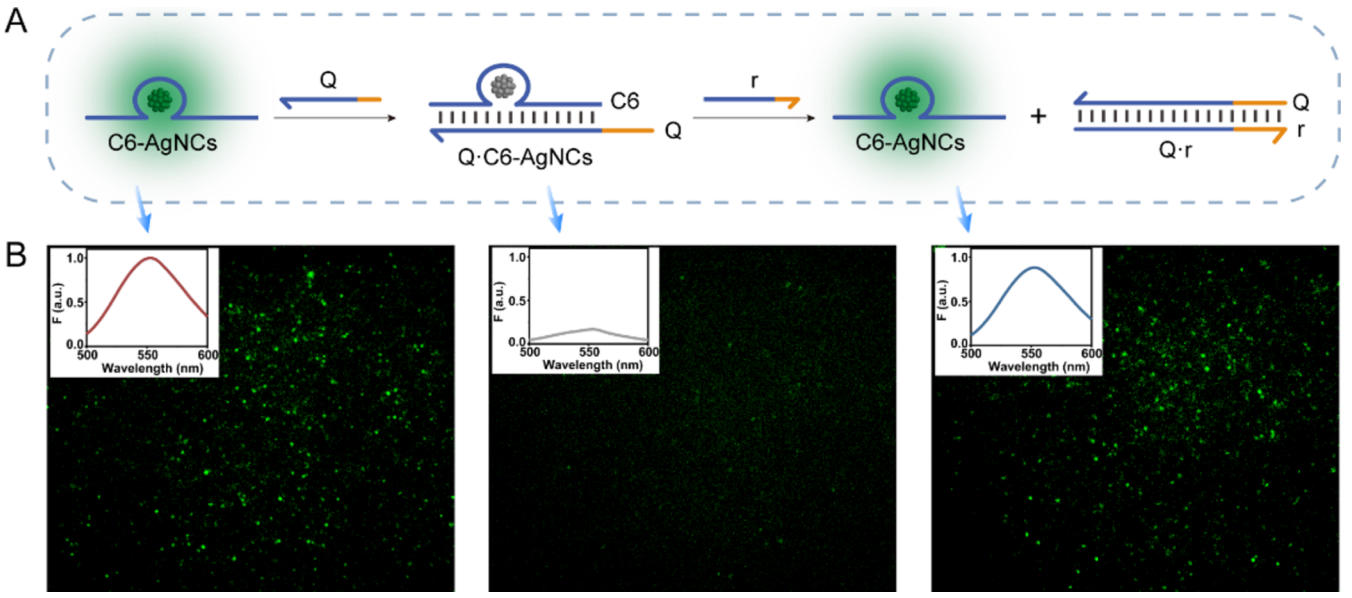

Figure 3. Fluorescence quenching and subsequent recovery of C6-AgNCs. (A) Schematic illustration depicting the process of fluorescence quenching and recovery of C6-AgNCs. (B) Total internal reflection fluorescence microscope images exhibiting C6-AgNCs, quenched C6-AgNCs, and recovered C6-AgNCs samples nonspecifically adsorbed onto a coverslip. Insets correspondingly display the fluorescence spectra of these AgNCs samples.

subsequent fluorescence restoration of the C6-AgNCs upon hybridization. By leveraging the amplification capability of CIDDC, we can achieve the sensitive detection of HBV DNA by monitoring the fluorescence restoration of C6-AgNCs, as explained above.

Construction of the Hybridization-Responsive DNA-AgNCs Reporter

In this work, a cytosine-rich domain-containing single-stranded DNA template, called C6, was utilized for the synthesis of fluorescent AgNCs. Due to the strong affinity between cytosine and Ag^+, silver ions preferentially bound to the cytosine bases within the cytosine-rich domain and were subsequently reduced to form AgNCs by $NaBH_4$ (see the Experimental Section for detailed procedures). The used DNA sequences are given in Table S1. The resultant DNA-AgNCs, named C6-AgNCs, displayed green fluorescence emission at 553 nm with an optimal excitation wavelength at 468 nm (Figure 1A). Notably, C6-AgNCs presented an excitation-wavelength-dependent fluorescence spectrum, which is a characteristic behavior commonly observed in ultrasmall AgNCs (Figure S1). The TEM image revealed that the C6-AgNCs exhibited high dispersion and had an average size of approximately 2 nm

https://doi.org/10.1021/jacsau.4c00291
JACS Au 2024, 4, 2323−2334

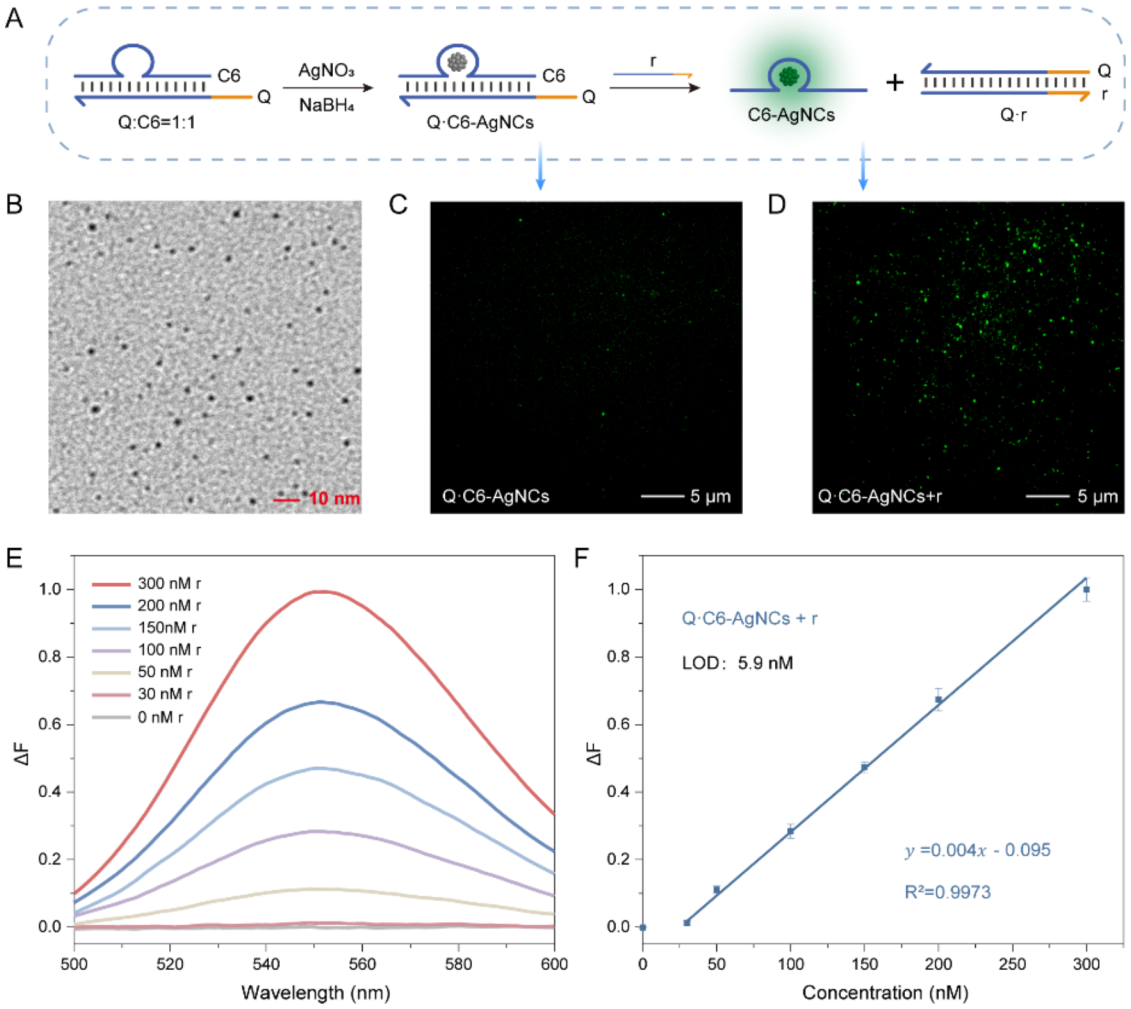

Figure 4. Fluorescence activation of Q·C6-AgNCs upon displacement of Q by r. (A) Schematic illustration depicting the synthesis of AgNCs using Q·C6 as a template and the fluorescence activation of Q·C6-AgNCs upon displacement of Q by r. (B) TEM image showcasing the morphology of Q·C6 templated AgNCs. (C, D) Total internal reflection fluorescence microscope images displaying Q·C6-AgNCs before and after activation with the r strand. (E) Changes in fluorescence spectra of 300 nM Q·C6-AgNCs upon the addition of the r strand at different concentrations (30, 50, 100, 150, 200, and 300 nM). (F) Linear relationship between ΔF (fluorescence intensity increment) and the concentration of r strand.

(Figure 1B). Fluorescence spectra of C6-AgNCs were measured at different reduction times to investigate the kinetics of C6-AgNCs growth (Figure 1C). As depicted in Figure 1D, the emission of C6-AgNCs at 553 nm became progressively stronger with increasing reduction time from 0 to 36 h and tended to get stable after 36 h. Therefore, a reduction time of 36 h was chosen for the synthesis of AgNCs to facilitate the subsequent construction of the sensing platform. In the absence of the C6 strand in the reaction system, the direct reduction of silver ions to fluorescent AgNCs by sodium borohydride did not occur (Figure S2). This observation further confirms the dependence of AgNCs generation on the presence of C6 as a template. The obtained C6-AgNCs are quite stable, with no fluorescence intensity decay observed after storage at 4 °C for 30 days (Figure S3).

Significantly, the DNA-AgNCs complex obtained by using DNA oligos as templates inherits the recognition abilities of the templates. Upon introducing the Q strand, C6 forms a partial duplex with Q through Watson−Crick base pairing (Figure 2A). As shown in Figure 2B, the fluorescence intensity of AgNCs at 553 nm decreased gradually with increasing concentrations of the Q strand. Interestingly, despite substantial fluorescence quenching, the morphology of the AgNCs remains largely unchanged. The Q·C6-AgNCs exhibited good dispersibility, and their particle size remains around 2 nm, similar to that of the C6-AgNCs (Figure 2C). The exact mechanism behind the fluorescence quenching of C6-AgNCs is not fully understood. However, it is hypothesized that the hybridization of C6 with Q is likely to cause changes in both the structure and composition of the template. These alterations impact the microenvironment (especially the adjacent bases) surrounding the AgNCs, ultimately leading to the quenching of fluorescence of the encapsulated AgNCs.

As there is a toehold at the 5′ terminal of the Q strand within the Q·C6 complex, the introduction of the r strand, which is the complementary strand of Q, initiates the TMSD reaction, resulting in the liberation and consequent fluorescence recovery of the C6-AgNCs (Figure 3A, schematic). As depicted in Figure 3B, the initially vibrant green fluorescence of C6-AgNCs diminishes upon the addition of an ample amount of Q. Nevertheless, when the r chain was added at an equivalent concentration as the Q chain, the fluorescence intensity of the AgNCs nearly restored to its prequenching level. The insets display the emission spectra of

https://doi.org/10.1021/jacsau.4c00291
JACS Au 2024, 4, 2323−2334

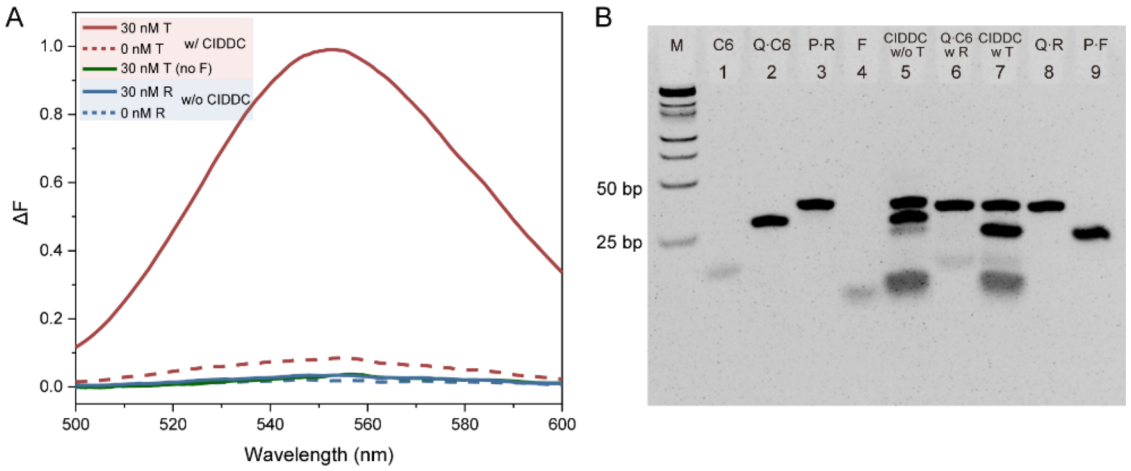

Figure 5. Feasibility and amplification effect of the CIDDC system. (A) Changes in fluorescence spectra of 300 nM Q·C6-AgNCs probe upon the addition of a 30 nM R strand without CIDDC or 30 nM HBV DNA (T strand) with CIDDC amplification. CIDDC system: 300 nM P·R and 3 μM F. ΔF represents the changes in fluorescent intensity observed in the 300 nM Q·C6-AgNCs probe with corresponding operations. (B) Results of native PAGE after DNA separation. Lanes: (1) 1 μM C6, (2) 1 μM Q·C6, (3) 1 μM P·R, (4) 1 μM F, (5) 1 μM Q·C6 + 1 μM P·R + 10 μM F, (6) 1 μM Q·C6 + 1 μM R, (7) 1 μM Q·C6 + 1 μM P·R + 10 μM F + 50 nM T, (8) 1 μM Q·R, (9) 1 μM P·F. All DNA components were mixed and incubated for 100 min electrophoretic separation.

C6-AgNCs under different conditions when excited at a wavelength of 468 nm. These findings further support the notion that the fluorescence quenching of C6-AgNCs is primarily attributed to changes in the structure and composition of the template.

Based on the aforementioned results, we have compelling evidence to suggest that the Q·C6 complex can effectively serve as a template for synthesizing quenched AgNCs, which fluoresces through the dissociation of the Q strand upon hybridization with the r strand (Figure 4A). Except for the initial step of C6 hybridizing with Q of the same concentration to form a partial duplex, all other steps and reaction conditions remain identical to those employed in the synthesis of AgNCs using C6 as the template. The successful formation of AgNCs with the Q·C6 template is indicated by the nanoparticles' average size of about 2 nm and their good dispersibility, as demonstrated by TEM analysis (Figure 4B). As anticipated, the addition of the r strand (complementary to the Q strand) results in the illumination of AgNCs, emitting a vibrant green glow (Figure 4C,D). Figure 4E shows the fluorescence intensity of the AgNCs reporter in response to various concentrations of the r strand (from 30 to 300 nM). It is evident that the fluorescence intensity of AgNCs gradually increases with progressive increment in r strand concentration. Notably, there exists a strong linear relationship between the increase in fluorescence intensity at 553 nm of AgNCs and the concentration of the r strand (Figure 4F). Additionally, the full spectrum scan graph depicting the changes in the activated AgNCs emission across various excitation wavelengths closely resembles that of the C6-AgNCs (Figure S4). When the r strand is utilized as a surrogate target, the as-prepared Q·C6 templated AgNCs (Q·C6-AgNCs) can be classified as a signal-on fluorescent reporter for the r strand, with a detection limit of 5.9 nM for the r strand.

Feasibility of HBV DNA Detection by Employing Q·C6-AgNCs as Reporter and CIDDC as Operational Amplifier

As mentioned earlier in the explanation of the detection principle, in order to enhance the sensitivity of the assay, we have architected a CIDDC, which functions as an operational amplifier to convert the input of the target strand (T strand, in this case, HBV DNA) into a large output of R strands. For a detailed description of the sequence and pairing information on DNA oligos, refer to Figure S5 and Table S1. The hybridization free energies of P·R, P·T, and P·F are deliberately tailored to be essentially equal (Figure S6). This CIDDC is composed of two initiating components, P·R and F. Upon the input of the target, this CIDDC undergoes two TMSD reactions: (I) P·R+T $\rightleftharpoons$ P·T+R and (II) P·T+F $\rightleftharpoons$ P·F+T. The hybridization free energy of P·R and P·T is equal, which leads to the generation of a corresponding amount of P·T when a certain amount of T strand is added, establishing equilibrium in reaction (I). However, owing to the equal hybridization free energy of P·T and P·F, when the initial concentration of F significantly exceeds that of T, it creates a concentration-disequilibrium driving force that effectively promotes the forward reaction P·T+F $\rightarrow$ P·F+T in reaction (II). This forward reaction (II) generates T while consuming P·T, which enables the recycling of T and pulling reaction (I) forward. By cascading and looping of these two TMSD reactions, the CIDDC system operates smoothly, ultimately resulting in the recycling of T and the generation of a large amount of R. The R strand incorporates the complete sequence of the r strand, which can subsequently illuminate the fluorescence of the Q·C6-AgNCs reporter.

To validate the feasibility and amplification effect of this CIDDC system, we subjected the system to a 30 nM target. The 300 nM as-prepared Q·C6-AgNCs were initially introduced into the system as reporter. As depicted in Figure 5A, it is evident that the implementation of the CIDDC system for a period of time (100 min) resulted in a significant increase in fluorescence intensity of the AgNCs reporter in the presence of the 30 nM target. In contrast, direct exposure to 30 nM R (surrogate target) had a minimal impact on the fluorescence intensity of the AgNCs reporter. Furthermore, in the absence of the fuel strand, even with the addition of a 30 nM target, there was negligible change in the fluorescence of the AgNCs. These results demonstrate the feasibility of the CIDDC design and its reliance on concentration imbalance driving. The

https://doi.org/10.1021/jacsau.4c00291
JACS Au 2024, 4, 2323−2334

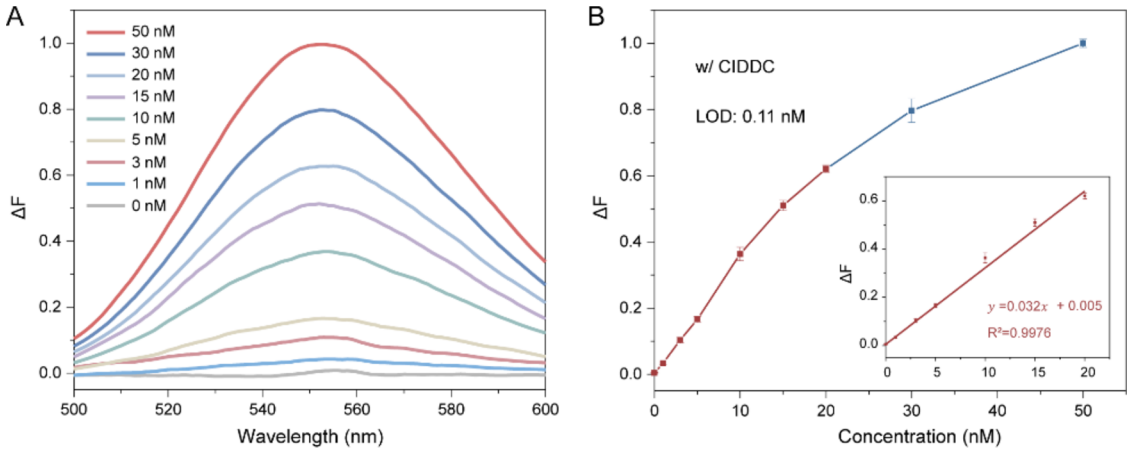

Figure 6. Detection of HBV DNA utilizing the Q·C6-AgNCs probe with the CIDDC system. (A) Fluorescence spectra changes of the 300 nM Q·C6-AgNCs probe upon the addition of HBV DNA at various concentrations (1, 3, 5, 10, 15, 20, 30, 50 nM), with the implementation of CIDDC. (B) Linear correlation between ΔF (fluorescence intensity increment) and the concentration of HBV DNA.

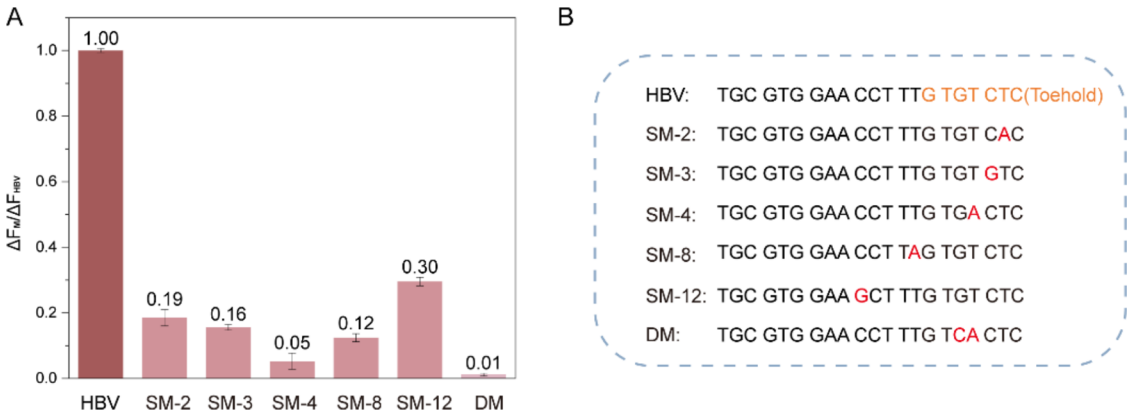

Figure 7. Specificity of the CIDDC-empowered sensing system. (A) Specificity of 300 nM Q·C6-AgNCs probe for 10 nM HBV DNA compared to other 10 nM mismatched DNAs, with the implementation of CIDDC. (B) Sequences of HBV and mismatched DNAs. SM-2, SM-3, SM-4, SM-8, and SM-12 indicate single mutation base at different sites, while DM represents two bases mismatch. The mutated bases are highlighted in red. ΔF_{HBV} and ΔF_{M} represent the changes in fluorescent intensity observed in the 300 nM Q·C6-AgNCs probe upon the addition of 10 nM HBV DNA and mismatched DNA with CIDDC amplification, respectively.

Native PAGE results further validate the feasibility of the CIDDC system. It is worth mentioning that due to the poor sensitivity of electrophoresis, we have accordingly increased the concentrations of various components: P·R and Q·C6 were 1 μM each, F was 10 μM, and T was 50 nM. Figure 5B reveals that the introduction of 50 nM T to the CIDDC system leads to the disappearance of Q·C6 and P·R bands, while Q·R, P·F, and C6 bands emerge (Lane7). This is because the presence of T initiates the catalytic cycle of CIDDC, leading to the consumption of F and P·R, generating P·F and R. Subsequently, R further reacts with Q·C6 through TMSD to produce Q·R and C6. Both fluorescence and electrophoresis results manifest the successful transformation and amplification of the input T strand into a substantial amount of the output R strand by this CIDDC system.

Performance of the CIDDC Coupled with Q·C6-AgNCs for HBV Detection

DNA computing showcases remarkable parallel computing capabilities. Therefore, in this study, we implemented a one-pot procedure that directly combines the Q·C6-AgNCs reporter with the CCIDC system from the outset. This approach enables simultaneous operation of the CCIDC process and the liberation and subsequent fluorescence recovery of AgNCs. Comparatively, the one-pot procedure exhibits higher execution efficiency and achieves a superior signal-to-noise ratio within the same reaction time when contrasted with the step-by-step procedure, where CIDDC is initially executed followed by the addition of the Q·C6-AgNCs reporter (Figure S7). This enhanced performance of the one-pot procedure primarily stems from DNA computing's inherent parallel computing capability. Furthermore, the subsequent TMSD reaction used to release the C6-AgNCs consumes the R strand, which serves as a drain on the upstream CIDDC. This effectively pulls the TMSD reaction (II) of the CIDDC forward, thus ultimately promoting the operation of the whole CIDDC system. In order to enhance the performance of this Q·C6-AgNCs coupled CIDDC platform for HBV detection, we optimized several reaction conditions with the signal-to-noise ratio (SNR = $\Delta F/\Delta F_0$) of the system serving as the guiding indicator. The optimization was conducted by using a 10 nM target concentration as the reference. As shown in Figure S8A,B, the optimum operation time for CIDDC was determined to be 100 min, while the optimal temperature was identified as 20 °C. Additionally, Figure S8C,D reveals that the optimal concentration ratios of F

https://doi.org/10.1021/jacsau.4c00291
JACS Au 2024, 4, 2323−2334

vs P·R and P vs R were established to 10:1 and 1.2:1, respectively.

We subsequently evaluated the performance of the CIDDC system coupled with a Q·C6-AgNC-based nanoprobe for quantitative analysis of HBV DNA under the selected optimum reaction conditions. Different concentrations of HBV DNA (T strand) were introduced into the CIDDC system containing 300 nM Q·C6-AgNCs reporter. As shown in Figure 6A, the green fluorescence emitted by the reporter was gradually intensified with the cumulative concentration of HBV DNA. Notably, a good linear correlation between the fluorescence intensity and the target DNA concentration was observed within the range of 1−20 nM (Figure 6B). Thanks to the amplification effect of CIDDC, the detection limit for the target DNA was improved to 0.11 nM, a significant enhancement compared to the 5.9 nM detection limit of the Q·C6-AgNCs reporter for the surrogate target (r strand). The sensitivity of the Q·C6-AgNC-based nanoprobe, aided by CIDDC, is either comparable to or superior to that of previously reported DNA-AgNC-based probes for nucleic acid detection (Table S2).

To further assess the specificity of this CIDDC-empowered sensing system, we subjected the system with similar DNA strands containing either only one (SM-2, SM-3, SM-4, SM-8, and SM-12) or two (DM) differential nucleotides compared to HBV DNA. The sequences of these DNAs are shown in Figure 7B. In the presence of a single-nucleotide mutation, the increase in fluorescence intensity of the AgNC reporter was approximately 5 to 30% of that induced by the same concentration of the HBV DNA target (Figure 7A). Different mutation sites within the DNA sequence resulted in varying degrees of interference. When the number of mutated bases increased to two, the signal variation of the AgNC reporter is negligible compared to the blank control. These results validate that our constructed sensing platform offers high specificity with single-base mismatch discriminability for HBV DNA detection. Here, the high specificity of our system is primarily attributed to the hindering effect of mismatches on the initial step of CIDDC, namely, the TMSD reaction between P·R and T. This hindrance occurs due to the equal hybridization free energy between P·R and P·T.

Given that blood transmission is the predominant route of HBV transmission, the detection of HBV DNA in blood is crucial for diagnosing HBV infection, monitoring treatment progress, and preventing further transmission. Consequently, we assessed the effectiveness of our method by detecting HBV DNA in the serum samples. To evaluate its performance, we conducted recovery experiments using 10-fold diluted healthy human serum samples spiked with three different concentrations of HBV DNA (10, 15, and 20 nM). Subsequently, we performed three repetitive experiments for each sample, employing our sensing platform. The results, as shown in Table 1, demonstrated recoveries ranging from 95.5 to 100.4% with relative standard deviations (RSDs) below 5.0%, suggesting great promise for the clinical applicability of our platform.

Table 1. Recoveries of HBV DNA in the Human Serum Samples (N = 3)

sample	added (nM)	detected (nM)	recovery (%)	RSD (%)
1	10	9.7	96.8	4.2
2	15	15.1	100.4	1.3
3	20	19.1	95.5	4.8

CONCLUSIONS

To summarize, we have successfully developed a novel enzyme-free fluorescence sensing platform for nucleic acid detection by leveraging CIDDC as a signal amplifier and customized hybridization-responsive DNA-AgNCs as a reporter. This mix-and-detection assay format is simple, performed isothermally, and exhibits high efficiency, making it affordable and viable for application in regions with high endemicity and limited resources. By incorporating the constructed CIDDC system, we have not only enhanced the sensitivity but also achieved high specificity in our method. Importantly, a notable advantage of this CIDDC system is its capability to convert and amplify the input DNA into enriched generic single-stranded DNA output through the implementation of a computational DNA circuit. Remarkably, the resulting output signal sequence bears no correlation whatsoever with the input DNA sequence (e.g., the sequences of "r" and "T" in this study). As a result, our method possesses high adaptability and universality, as it can be applied to detect various targets by simply adjusting the sequences of target-related nucleic acid components within the CIDDC system. Furthermore, different CIDDC systems can operate in parallel, enabling the simultaneous detection of multiple targets in a single run. Moreover, this CIDDC system can be easily cascaded with other enzyme-based or DNA circuit-based amplification methods, offering a versatile and adaptable approach for nucleic acid detection. Given the aforementioned advantages, this CIDDC-empowered platform holds great promise for biomedical and clinical applicability.

EXPERIMENTAL SECTION

Materials and Apparatus

All oligonucleotides were synthesized by Sangon Biotech (Shanghai, China). Silver nitrate ($AgNO_3$, >99%) was purchased from Sigma-Aldrich Co., Ltd. (Shanghai, China). Sodium borohydride ($NaBH_4$, 98%) was obtained from Shanghai Aladdin Biochemical Technology Co., Ltd. (Shanghai, China). Healthy human serum was sourced from Shanghai Jiwei Biotechnology Co., Ltd. (Shanghai, China). Tris(hydroxymethyl) aminomethane (Tris), boric acid (H_3BO_3), ethylenediaminetetraacetic acid disodium salt dihydrate ($Na_2EDTA{\cdot}2H_2O$), and magnesium acetate tetrahydrate ($((CH_3COO)_2Mg{\cdot}4H_2O$) were obtained from Sinopharm Chemical Reagent Co., Ltd. (Shanghai, China). Acetic acid (CH_3COOH), DNA Marker (25−500 bp), acryl/bis 30% Solution (19:1), ammonium persulfate (APS), *N*,*N*,*N*′,*N*′-tetramethylethylenediamine (TEMED), 4S Gel-red (10 000× in water), and 6× Ficoll Gel Loading Buffer were purchased from Sangon Biotech Co., Ltd. (Shanghai, China). All reagents were of analytical grade and used without further purification. Aqueous solutions were prepared using ultrapure water (>18 MΩ·cm) obtained from the Millipore water purification system.

Fluorescence spectra were obtained using a FluoroMax Plus Fluorescence Spectrophotometer (HORIBA Scientific, Japan). Both the excitation and emission slit widths were set at 5 nm. Fluorescence imaging was performed using total internal reflection microscopy (TIRFM) with a 100× objective lens (Nikon, Japan). The synthesized DNA-AgNCs were characterized by transmission electron microscopy (TEM) using a Hitachi H-7500 instrument. Gel images were captured using the GBOX-F3-E system (Gene Company Limited). The pH of the buffers was monitored using a PB-10 pH meter (Sartorius, Germany).

Buffer Conditions

The buffer solution used for synthesizing DNA-AgNCs was 1× TAE-Mg (40 mM Tris, 30 mM CH_3COOH, 2 mM EDTA, 12.5 mM

https://doi.org/10.1021/jacsau.4c00291
JACS Au 2024, 4, 2323−2334

$(CH_3COO)_2Mg$, pH = 7.5). For all hybridization reactions, the buffer solution employed was 1× TAE-Mg (40 mM Tris, 22.5 mM CH_3COOH, 2 mM EDTA, 12.5 mM $(CH_3COO)_2Mg$, pH = 8.0). The electrolyte used in PAGE was 1× TBE-Mg (40 mM Tris, 20 mM H_3BO_3, 2 mM EDTA, 12.5 mM $(CH_3COO)_2Mg$).

Synthesis of DNA-AgNCs

DNA-AgNCs were synthesized and stabilized in an aqueous solution by using DNA scaffolds containing six consecutive cytosines (C6 domain). In brief, two single-stranded DNAs (C6 and Q) at equal concentrations were dissolved in 1× TAE-Mg buffer (pH = 7.5) and then annealed from 95 to 4 °C to form duplex Q·C6. Subsequently, $AgNO_3$ was added to the Q·C6 solutions and reduced by $NaBH_4$ (molar ratio, dsDNA/$AgNO_3$/$NaBH_4$ = 1:6:6), resulting in the formation of Q·C6-AgNCs. The synthesis process of C6-AgNCs followed the same procedural steps, with the only difference being the use of a single-stranded C6 as a template instead.

Quenching the Fluorescence of C6-AgNCs upon Hybridization with Q Strand

The synthesized C6-AgNCs (300 nM) were hybridized with various concentrations of Q in 1× TAE-Mg (pH = 8.0). After incubation at 20 °C for 100 min, the fluorescence intensity of the mixture was measured at excitation/emission wavelengths of 468/553 nm.

DNA Detection Using the Customized Q·C6-AgNCs without the Assistance of CIDDC

The as-prepared Q·C6-AgNCs (300 nM) were hybridized with various concentrations of r in 1× TAE-Mg buffer (pH = 8.0). After incubation at 20 °C for 40 min, the fluorescence intensity of the mixture was measured at excitation/emission wavelengths of 468/553 nm.

Detection of HBV DNA Using the Q·C6-AgNCs Probe with the Implementation of CIDDC

Different concentrations of T (HBV DNA) were added to a mixture containing 1× TAE-Mg buffer (pH = 8.0), 300 nM P·R (P and R were dissolved in 1× TAE-Mg at pH = 8.0 and annealed from 95 to 4 °C to form the P·R duplex), 3 μM F, and 300 nM Q·C6-AgNCs. After incubating the mixture at 20 °C for 100 min, the fluorescence intensity was measured at excitation/emission wavelengths of 468/553 nm. To assess the specificity of our method, we challenged the system with similar DNA strands containing either only one or two differential nucleotides compared to HBV DNA at a concentration of 10 nM.

Polyacrylamide Gel Electrophoresis (PAGE) Characterization

The feasibility of CIDDC in HBV DNA detection was demonstrated using PAGE. In detail, the gel was run in 10% acrylamide solution with 1× TBE-Mg buffer at 80 V constant voltage for 100 min at room temperature. Then, the gel was stained with Gel-Red for 10 min to indicate the position of DNA and photographed. At this point, we increased the corresponding concentrations of the various DNA elements as follows: P·R and Q·C6 at 1 μM each, F at 10 μM, and T at 50 nM.

■ ASSOCIATED CONTENT

Supporting Information

The Supporting Information is available free of charge at https://pubs.acs.org/doi/10.1021/jacsau.4c00291.

Fluorescence spectra of different DNA-AgNCs, stability of C6-AgNCs, optimization of CIDDC reaction conditions (e.g., operational process, reaction temperature, reaction time, and concentration ratios of each component), and the sequences and pairing information on the DNA utilized in this study (Figures S1−S7) (Tables S1 and S2) (PDF)

■ AUTHOR INFORMATION

Corresponding Authors

Shao Su − *State Key Laboratory of Organic Electronics and Information Displays and Jiangsu Key Laboratory for Biosensors, Institute of Advanced Materials (IAM), Nanjing University of Posts and Telecommunications, Nanjing 210023, China;* orcid.org/0000-0002-9399-8249; Email: iamssu@njupt.edu.cn

Changfeng Zhu − *Department of Gastroenterology and Hepatology, Zhongshan Hospital, Fudan University, Shanghai 200032, China; Shanghai Institute of Liver Diseases, Shanghai 200032, China;* orcid.org/0000-0002-4922-0659; Email: zhuchangfeng@fudan.edu.cn

Authors

Suo Lv − *State Key Laboratory of Organic Electronics and Information Displays and Jiangsu Key Laboratory for Biosensors, Institute of Advanced Materials (IAM), Nanjing University of Posts and Telecommunications, Nanjing 210023, China*

Qunyan Yao − *Department of Gastroenterology and Hepatology, Zhongshan Hospital, Fudan University, Shanghai 200032, China; Department of Gastroenterology and Hepatology, Zhongshan Hospital (Xiamen), Fudan University, Xiamen 361015, China; Shanghai Geriatric Medical Center, Shanghai 201104, China*

Jiasheng Yi − *State Key Laboratory of Organic Electronics and Information Displays and Jiangsu Key Laboratory for Biosensors, Institute of Advanced Materials (IAM), Nanjing University of Posts and Telecommunications, Nanjing 210023, China*

Jingyi Si − *Department of Gastroenterology and Hepatology, Zhongshan Hospital, Fudan University, Shanghai 200032, China*

Yifan Gao − *Department of Gastroenterology and Hepatology, Zhongshan Hospital, Fudan University, Shanghai 200032, China*

Complete contact information is available at: https://pubs.acs.org/10.1021/jacsau.4c00291

Author Contributions

#S.L. and Q.Y. contributed equally to this work. CRediT: **Suo Lv** conceptualization, data curation, investigation, methodology, validation, writing-original draft; **Qunyan Yao** funding acquisition, investigation, writing-original draft; **Jiasheng Yi** investigation, methodology, resources; **Jingyi Si** investigation, methodology; **Yifan Gao** investigation, software; **Shao Su** project administration, resources, supervision, writing-review & editing; **Changfeng Zhu** conceptualization, funding acquisition, project administration, supervision, writing-review & editing.

Notes

The authors declare no competing financial interest.

■ ACKNOWLEDGMENTS

This work was supported by the National Natural Science Foundation of China (no. 22274029); the Science and Technology Commission of Shanghai Municipality (nos. 22ZR1412000, 22140900700, 23ZR1411300); and Postgraduate Research & Practice Innovation Program of Jiangsu Province (no. SJCX22_0252).

REFERENCES

(1) Sheena, B. S.; Hiebert, L.; Han, H.; Ippolito, H.; Abbasi-Kangevari, M.; Abbasi-Kangevari, Z.; Abbastabar, H.; Abdoli, A.; Abubaker Ali, H.; Adane, M. M.; Adegboye, O. A.; Adnani, Q. E. S.; Advani, S. M.; Afzal, M. S.; Afzal, S.; Aghaie Meybodi, M.; Ahadinezhad, B.; Ahinkorah, B. O.; Ahmad, S.; Ahmad, T.; Ahmadi, S.; Ahmed, H.; Ahmed, M. B.; Ahmed Rashid, T.; Akalu, G. T.; Aklilu, A.; Akram, T.; Al Hamad, H.; Alahdab, F.; Alem, A. Z.; Alem, D. T.; Alhalaiqa, F. A. N.; Alhassan, R. K.; Ali, L.; Ali, M. A.; Alimohamadi, Y.; Alipour, V.; Alkhayyat, M.; Almustanyir, S.; Al-Raddadi, R. M.; Altawalah, H.; Amini, S.; Amu, H.; Ancuceanu, R.; Andrei, C. L.; Andrei, T.; Anoushiravani, A.; Ansar, A.; Anyasodor, A. E.; Arabloo, J.; Arab-Zozani, M.; Argaw, A. M.; Argaw, Z. G.; Arshad, M.; Artamonov, A. A.; Ashraf, T.; Atlaw, D.; Ausloos, F.; Ausloos, M.; Azadnajafabad, S.; Azangou-Khyavy, M.; Azari Jafari, A.; Azarian, G.; Bagheri, S.; Bahadory, S.; Baig, A. A.; Banach, M.; Barati, N.; Barrow, A.; Batiha, A.-M. M.; Bejarano Ramirez, D. F.; Belgaumi, U. I.; Berhie, A. Y.; Bhagat, D. S.; Bhardwaj, N.; Bhardwaj, P.; Bhattacharyya, K.; Bhojaraja, V. S.; Bijani, A.; Biondi, A.; Bodicha, B. B. A.; Bojia, H. A.; Boloor, A.; Bosetti, C.; Braithwaite, D.; Briko, N. I.; Butt, Z. A.; Cámera, L. A.; Chakinala, R. C.; Chakraborty, P. A.; Charan, J.; Chen, S.; Choi, J.-Y. J.; Choudhari, S. G.; Chowdhury, F. R.; Chu, D.-T.; Chung, S.-C.; Cortesi, P. A.; Cowie, B. C.; Culbreth, G. T.; Dadras, O.; Dai, X.; Dandona, L.; Dandona, R.; De la Hoz, F. P.; Debela, S. A.; Dedefo, M. G.; Demeke, F. M.; Demie, T. G. G.; Demissie, G. D.; Derbew Molla, M.; Desta, A. A.; Dhamnetiya, D.; Dhimal, M. L.; Dhimal, M.; Didehdar, M.; Doan, L. P.; Dorostkar, F.; Drake, T. M.; Eghbalian, F.; Ekholuenetale, M.; El Sayed, I.; El Sayed Zaki, M.; Elhadi, M.; Elmonem, M. A.; Elsharkawy, A.; Enany, S.; Enyew, D. B.; Erkhembayar, R.; Eskandarieh, S.; Esmaeilzadeh, F.; Ezzikouri, S.; Farrokhpour, H.; Fetensa, G.; Fischer, F.; Foroutan, M.; Gad, M. M.; Gaidhane, A. M.; Gaidhane, S.; Galles, N. C.; Gallus, S.; Gebremeskel, T. G.; Gebreyohannes, E. A.; Ghadiri, K.; Ghaffari, K.; Ghafourifard, M.; Ghamari, S.-H.; Ghashghaee, A.; Gholami, A.; Gholizadeh, A.; Gilani, A.; Goel, A.; Golechha, M.; Goleij, P.; Golinelli, D.; Gorini, G.; Goshu, Y. A.; Griswold, M. G.; Gubari, M. I. M.; Gupta, B.; Gupta, S.; Gupta, V. B.; Gupta, V. K.; Haddadi, R.; Halwani, R.; Hamid, S. S.; Hamidi, S.; Hanif, A.; Haque, S.; Harapan, H.; Hargono, A.; Hariri, S.; Hasaballah, A. I.; Hasan, S. M. M.; Hassanipour, S.; Hassankhani, H.; Hay, S. I.; Hayat, K.; Heidari, G.; Herteliu, C.; Heyi, D. Z.; Hezam, K.; Holla, R.; Hosseini, M.-S.; Hosseini, M.; Hosseinzadeh, M.; Hostiuc, M.; Househ, M.; Huang, J.; Hussein, N. R.; Iavicoli, I.; Ibitoye, S. E.; Ilesanmi, O. S.; Ilic, I. M.; Ilic, M. D.; Irham, L. M.; Islam, J. Y.; Ismail, N. E.; Jacobsen, K. H.; Jadidi-Niaragh, F.; Javadi Mamaghani, A.; Jayaram, S.; Jayawardena, R.; Jebai, R.; Jha, R. P.; Joseph, N.; Joukar, F.; Kaambwa, B.; Kabir, A.; Kabir, Z.; Kalhor, R.; Kandel, H.; Kanko, T. K. T.; Kantar, R. S.; Karaye, I. M.; Kassa, B. G.; Kemp Bohan, P. M.; Keykhaei, M.; Khader, Y. S.; Khajuria, H.; Khan, G.; Khan, I. A.; Khan, J.; Khan, M. A. B.; Khanali, J.; Khater, A. M.; Khatib, M. N.; Khodadost, M.; Khoja, A. T.; Khosravizadeh, O.; Khubchandani, J.; Kim, G. R.; Kim, H.; Kim, M. S.; Kim, Y. J.; Kocarnik, J. M.; Kolahi, A.-A.; Koteeswaran, R.; Kumar, G. A.; La Vecchia, C.; Lal, D. K.; Landires, I.; Lasrado, S.; Lazarus, J. V.; Ledda, C.; Lee, D. W.; Lee, S.-w.; Lee, Y. Y.; Levi, M.; Li, J.; Lim, S. S.; Lobo, S. W.; Lopukhov, P. D.; Loureiro, J. A.; MacLachlan, J. H.; Magdy Abd El Razek, H.; Magdy Abd El Razek, M.; Majeed, A.; Makki, A.; Malekpour, M.-R.; Malekzadeh, R.; Malik, A. A.; Mansour-Ghanaei, F.; Mansournia, M. A.; Martins-Melo, F. R.; Matthews, P. C.; Mendoza, W.; Menezes, R. G.; Meretoja, T. J.; Mersha, A. G.; Mestrovic, T.; Miller, T. R.; Minh, L. H. N.; Mirica, A.; Mirmoeeni, S.; Mirrakhimov, E. M.; Misra, S.; Mithra, P.; Moazen, B.; Mohamadkhani, A.; Mohammadi, M.; Mohammed, S.; Moka, N.; Mokdad, A. H.; Moludi, J.; Momtazmanesh, S.; Monasta, L.; Moradi, G.; Moradzadeh, M.; Moradzadeh, R.; Moraga, P.; Mostafavi, E.; Mubarik, S.; Muniyandi, M.; Murray, C. J. L.; Naghavi, M.; Naimzada, M. D.; Narasimha Swamy, S.; Natto, Z. S.; Nayak, B. P.; Nazari, J.; Negoi, I.; Negru, S. M.; Nejadghaderi, S. A.; Neupane Kandel, S.; Nguyen, H. L. T.; Ngwa, C. H.; Niazi, R. K.; Nnaji, C. A.; Noubiap, J. J.; Nowroozi, A.; Nuñez-Samudio, V.; Oancea, B.; Ochir, C.; Odukoya, O. O.; Oh, I.-H.; Olagunju, A. T.; Olakunde, B. O.; Omar Bali, A.; Omer, E.; Otstavnov, S. S.; Oumer, B.; Padubidri, J. R.; Pana, A.; Pandey, A.; Park, E.-C.; Pashazadeh Kan, F.; Patel, U. K.; Paudel, U.; Petcu, I.-R.; Piracha, Z. Z.; Pollok, R. C. G.; Postma, M. J.; Pourshams, A.; Poustchi, H.; Rabiee, M.; Rabiee, N.; Rafiei, A.; Rafiei, S.; Raghuram, P. M.; Rahman, M.; Rahmani, A. M.; Rahmawaty, S.; Rajesh, A.; Ranasinghe, P.; Rao, C. R.; Rao, S. J.; Rashidi, M.; Rashidi, M.-M.; Rawaf, D. L.; Rawaf, S.; Rawassizadeh, R.; Rezaei, N.; Rezapour, A.; Rezazadeh-Khadem, S.; Rodriguez, J. A. B.; Rwegerera, G. M.; Sabour, S.; Saddik, B.; Saeb, M. R.; Saeed, U.; Sahebkar, A.; Saif-Ur-Rahman, K. M.; Salahi, S.; Salimzadeh, H.; Sampath, C.; Samy, A. M.; Sanabria, J.; Sanmarchi, F.; Santric-Milicevic, M. M.; Sarveazad, A.; Sathian, B.; Sawhney, M.; Seidu, A.-A.; Sepanlou, S. G.; Seylani, A.; Shahabi, S.; Shaikh, M. A.; Shaker, E.; Shakhmardanov, M. Z.; Shannawaz, M.; Shenoy, S. M.; Shetty, J. K.; Shetty, P. H.; Shibuya, K.; Shin, J. I.; Shobeiri, P.; Sibhat, M. M.; Singh, A. D.; Singh, J. A.; Singh, S.; Skryabin, V. Y.; Skryabina, A. A.; Sohrabpour, A. A.; Song, S.; Tabaeian, S. P.; Tadesse, E. G.; Taheri, M.; Tampa, M.; Tan, K.-K.; Tavakoli, A.; Tbakhi, A.; Tefera, B. N.; Tehrani-Banihashemi, A.; Tesfaw, H. M.; Thapar, R.; Thavamani, A.; Tohidast, S. A.; Tollosa, D. N.; Tosti, M. E.; Tovani-Palone, M. R.; Traini, E.; Tran, M. T. N.; Trihandini, I.; Tusa, B. S.; Ullah, I.; Vacante, M.; Valadan Tahbaz, S.; Valdez, P. R.; Varthya, S. B.; Vo, B.; Waheed, Y.; Weldesenbet, A. B.; Woldemariam, M.; Xu, S.; Yahyazadeh Jabbari, S. H.; Yaseri, M.; Yeshaw, Y.; Yiğit, V.; Yirdaw, B. W.; Yonemoto, N.; Yu, C.; Yunusa, I.; Zahir, M.; Zaki, L.; Zamani, M.; Zamanian, M.; Zastrozhin, M. S.; Vos, T.; Ward, J. W.; Dirac, M. A. Global, Regional, and National Burden of Hepatitis B, 1990−2019: A Systematic Analysis for the Global Burden of Disease Study 2019. *Lancet Gastroenterol. Hepatol.* **2022**, *7*, 796−829.

(2) Razavi-Shearer, D.; Gamkrelidze, I.; Pan, C.; Jia, J.; Berg, T.; Gray, R.; Lim, Y.-S.; Chen, C.-J.; Ocama, P.; Desalegn, H.; Abbas, Z.; Abdallah, A.; Aghemo, A.; Ahmadbekova, S.; Ahn, S. H.; Aho, I.; Akarca, U.; Al Masri, N.; Alalwan, A.; Alavian, S.; Al-Busafi, S.; Aleman, S.; Alfaleh, F.; Alghamdi, A.; Al-Hamoudi, W.; Aljumah, A.; Al-Naamani, K.; Al-Rifai, A.; Alserkal, Y.; Altraif, I.; Amarsanaa, J.; Anderson, M.; Andersson, M.; Armstrong, P.; Asselah, T.; Athanasakis, K.; Baatarkhuu, O.; Ben-Ari, Z.; Bensalem, A.; Bessone, F.; Biondi, M.; Bizri, A. R.; Blach, S.; Braga, W.; Brandão-Mello, C.; Brosgart, C.; Brown, K.; Brown, R., Jr; Bruggmann, P.; Brunetto, M.; Buti, M.; Cabezas, J.; Casanovas, T.; Chae, C.; Chan, H. L. Y.; Cheinquer, H.; Chen, P.-J.; Cheng, K. J.; Cheon, M.-E.; Chien, C.-H.; Choudhuri, G.; Christensen, P. B.; Chuang, W.-L.; Chulanov, V.; Cisneros, L.; Coffin, C.; Contreras, F.; Coppola, N.; Cornberg, M.; Cowie, B.; Cramp, M.; Craxi, A.; Crespo, J.; Cui, F.; Cunningham, C.; Dalgard, O.; De Knegt, R.; De Ledinghen, V.; Dore, G.; Drazilova, S.; Duberg, A.-S.; Egeonu, S.; Elbadri, M.; El-Kassas, M.; El-Sayed, M.; Estes, C.; Etzion, O.; Farag, E.; Ferradini, L.; Ferreira, P.; Flisiak, R.; Forns, X.; Frankova, S.; Fung, J.; Gane, E.; Garcia, V.; García-Samaniego, J.; Gemilyan, M.; Genov, J.; Gheorghe, L.; Gholam, P.; Gish, R.; Goleij, P.; Gottfredsson, M.; Grebely, J.; Gschwantler, M.; Guingane, N. A.; Hajarizadeh, B.; Hamid, S.; Hamoudi, W.; Harris, A.; Hasan, I.; Hatzakis, A.; Hellard, M.; Hercun, J.; Hernandez, J.; Hockicková, I.; Hsu, Y.-C.; Hu, C.-C.; Husa, P.; Janicko, M.; Janjua, N.; Jarcuska, P.; Jaroszewicz, J.; Jelev, D.; Jeruma, A.; Johannessen, A.; Kåberg, M.; Kaita, K.; Kaliaskarova, K.; Kao, J.-H.; Kelly-Hanku, A.; Khamis, F.; Khan, A.; Kheir, O.; Khoudri, I.; Kondili, L.; Konysbekova, A.; Kristian, P.; Kwon, J.; Lagging, M.; Laleman, W.; Lampertico, P.; Lavanchy, D.; Lázaro, P.; Lazarus, J. V.; Lee, A.; Lee, M.-H.; Liakina, V.; Lukšić, B.; Malekzadeh, R.; Malu, A.; Marinho, R.; Mendes-Correa, M. C.; Merat, S.; Meshesha, B. R.; Midgard, H.; Mohamed, R.; Mokhbat, J.; Mooneyhan, E.; Moreno, C.; Mortgat, L.; Müllhaupt, B.; Musabaev, E.; Muyldermans, G.; Naveira, M.; Negro, F.; Nersesov, A.; Nguyen, V. T. T.; Ning, Q.; Njouom, R.; Ntagirabiri, R.; Nurmatov, Z.; Oguche, S.; Omuemu, C.; Ong, J.; Opare-Sem, O.; Örmeci, N.; Orrego, M.; Osiowy, C.; Papatheodoridis, G.; Peck-Radosavljevic, M.; Pessoa, M.; Pham, T.; Phillips, R.; Pimenov, N.; Pincay-Rodríguez, L.; Plaseska-Karanfilska, D.; Pop, C.; Poustchi, H.; Prabdial-Sing, N.; Qureshi, H.; Ramji, A.; Rautiainen, H.; Razavi-

https://doi.org/10.1021/jacsau.4c00291
JACS Au 2024, 4, 2323−2334

Shearer, K.; Remak, W.; Ribeiro, S.; Ridruejo, E.; Ríos-Hincapié, C.; Robalino, M.; Roberts, L.; Roberts, S.; Rodríguez, M.; Roulot, D.; Rwegasha, J.; Ryder, S.; Sadirova, S.; Saeed, U.; Safadi, R.; Sagalova, O.; Said, S.; Salupere, R.; Sanai, F.; Sanchez-Avila, J. F.; Saraswat, V.; Sargsyants, N.; Sarrazin, C.; Sarybayeva, G.; Schréter, I.; Seguin-Devaux, C.; Seto, W.-K.; Shah, S.; Sharara, A.; Sheikh, M.; Shouval, D.; Sievert, W.; Simojoki, K.; Simonova, M.; Sinn, D. H.; Sonderup, M.; Sonneveld, M.; Spearman, C. W.; Sperl, J.; Stauber, R.; Stedman, C.; Sypsa, V.; Tacke, F.; Tan, S.-S.; Tanaka, J.; Tergast, T.; Terrault, N.; Thompson, A.; Thompson, P.; Tolmane, I.; Tomasiewicz, K.; Tsang, T.-Y.; Uzochukwu, B.; Van Welzen, B.; Vanwolleghem, T.; Vince, A.; Voeller, A.; Waheed, Y.; Waked, I.; Wallace, J.; Wang, C.; Weis, N.; Wong, G.; Wong, V.; Wu, J.-C.; Yaghi, C.; Yesmembetov, K.; Yip, T.; Yosry, A.; Yu, M.-L.; Yuen, M.-F.; Yurdaydin, C.; Zeuzem, S.; Zuckerman, E.; Razavi, H. Global Prevalence, Cascade of Care, and Prophylaxis Coverage of Hepatitis B in 2022: A Modelling Study. *Lancet Gastroenterol. Hepatol.* **2023**, *8*, 879−907.

(3) Jeng, W.-J.; Papatheodoridis, G. V.; Lok, A. S. F. Hepatitis B. *Lancet* **2023**, *401*, 1039−1052.

(4) Hepatitis B. https://www.who.int/news-room/fact-sheets/detail/hepatitis-b (accessed May 3, 2024).

(5) Chu, C.-J.; Lok, A. S.-F. Clinical Utility in Quantifying Serum HBV DNA Levels Using PCR Assays. *J. Hepatol.* **2002**, *36*, 549−551.

(6) Kessler, H. H.; Preininger, S.; Stelzl, E.; Daghofer, E.; Santner Brigitte, I.; Marth, E.; Lackner, H.; Stauber Rudolf, E. Identification of Different States of Hepatitis B Virus Infection with a Quantitative PCR Assay. *Clin. Diagn. Lab. Immunol.* **2000**, *7*, 298−300.

(7) Nguyen, M. H.; Wong, G.; Gane, E.; Kao, J.-H.; Dusheiko, G. Hepatitis B Virus: Advances in Prevention, Diagnosis, and Therapy. *Clin. Microbiol. Rev.* **2020**, *33*, No. e00046-19.

(8) Li, M.; Yin, F.; Song, L.; Mao, X.; Li, F.; Fan, C.; Zuo, X.; Xia, Q. Nucleic Acid Tests for Clinical Translation. *Chem. Rev.* **2021**, *121*, 10469−10558.

(9) Zhao, Y.; Chen, F.; Li, Q.; Wang, L.; Fan, C. Isothermal Amplification of Nucleic Acids. *Chem. Rev.* **2015**, *115*, 12491−12545.

(10) Wegner, K. D.; Hildebrandt, N. Quantum Dots: Bright and Versatile in Vitro and in Vivo Fluorescence Imaging Biosensors. *Chem. Soc. Rev.* **2015**, *44*, 4792−4834.

(11) Ma, Y.; Song, M.; Li, L.; Lao, X.; Wong, M.-C.; Hao, J. Advances in Upconversion Luminescence Nanomaterial-Based Biosensor for Virus Diagnosis. *Exploration* **2022**, *2*, No. 20210216.

(12) Tao, Y.; Li, M.; Ren, J.; Qu, X. Metal Nanoclusters: Novel Probes for Diagnostic and Therapeutic Applications. *Chem. Soc. Rev.* **2015**, *44*, 8636−8663.

(13) Liu, J. DNA-Stabilized, Fluorescent, Metal Nanoclusters for Biosensor Development. *TrAC, Trends Anal. Chem.* **2014**, *58*, 99−111.

(14) Ouyang, X.; Jia, N.; Luo, J.; Li, L.; Xue, J.; Bu, H.; Xie, G.; Wan, Y. DNA Nanoribbon-Assisted Intracellular Biosynthesis of Fluorescent Gold Nanoclusters for Cancer Cell Imaging. *JACS Au* **2023**, *3*, 2566−2577.

(15) Li, W.; Xie, H.; Gou, L.; Zhou, Y.; Wang, H.; Li, R.; Zhang, Y.; Liu, S.; Liu, J.; Lu, Y.; He, Z. E.; Chen, N.; Li, J.; Zhu, Y.; Wang, C.; Lv, M. DNA-Based Hydrogels with Multidrug Sequential Release for Promoting Diabetic Wound Regeneration. *JACS Au* **2023**, *3*, 2597−2608.

(16) Liu, S.; Yan, Q.; Cao, S.; Wang, L.; Luo, S.-H.; Lv, M. Inhibition of Bacteria in Vitro and in Vivo by Self-Assembled DNA-Silver Nanocluster Structures. *ACS Appl. Mater. Interfaces* **2022**, *14*, 41809−41818.

(17) Ouyang, X.; Wang, M.; Guo, L.; Cui, C.; Liu, T.; Ren, Y.; Zhao, Y.; Ge, Z.; Guo, X.; Xie, G.; Li, J.; Fan, C.; Wang, L. DNA Nanoribbon-Templated Self-Assembly of Ultrasmall Fluorescent Copper Nanoclusters with Enhanced Luminescence. *Angew. Chem., Int. Ed.* **2020**, *59*, 11836−11844.

(18) Yang, M.; Zhu, L.; Yang, W.; Xu, W. Nucleic Acid-Templated Silver Nanoclusters: A Review of Structures, Properties, and Biosensing Applications. *Coord. Chem. Rev.* **2023**, *491*, No. 215247.

(19) Chen, Y.; Phipps, M. L.; Werner, J. H.; Chakraborty, S.; Martinez, J. S. DNA Templated Metal Nanoclusters: From Emergent Properties to Unique Applications. *Acc. Chem. Res.* **2018**, *51*, 2756−2763.

(20) Guo, Y.; Pan, X.; Zhang, W.; Hu, Z.; Wong, K.-W.; He, Z.; Li, H.-W. Label-Free Probes Using DNA-Templated Silver Nanoclusters as Versatile Reporters. *Biosens. Bioelectron.* **2020**, *150*, No. 111926.

(21) Yeh, H.-C.; Sharma, J.; Han, J. J.; Martinez, J. S.; Werner, J. H. A DNA−Silver Nanocluster Probe That Fluoresces Upon Hybridization. *Nano Lett.* **2010**, *10*, 3106−3110.

(22) Zhou, W.; Zhu, J.; Fan, D.; Teng, Y.; Zhu, X.; Dong, S. A Multicolor Chameleon DNA-Templated Silver Nanocluster and Its Application for Ratiometric Fluorescence Target Detection with Exponential Signal Response. *Adv. Funct. Mater.* **2017**, *27*, No. 1704092.

(23) Zhang, Y.; Zhu, C.; Zhang, L.; Tan, C.; Yang, J.; Chen, B.; Wang, L.; Zhang, H. DNA-Templated Silver Nanoclusters for Multiplexed Fluorescent DNA Detection. *Small* **2015**, *11*, 1385−1389.

(24) Zhang, Y.; Mu, F.; Duan, Y.; Li, Q.; Pan, Y.; Du, H.; He, P.; Shen, X.; Luo, Z.; Zhu, C.; Wang, L. Label-Free Analysis of H5N1 Virus Based on Three-Segment Branched DNA-Templated Fluorescent Silver Nanoclusters. *ACS Appl. Mater. Interfaces* **2020**, *12*, 48357−48362.

(25) Zhang, J.; Li, C.; Zhi, X.; Ramón, G. A.; Liu, Y.; Zhang, C.; Pan, F.; Cui, D. Hairpin DNA-Templated Silver Nanoclusters as Novel Beacons in Strand Displacement Amplification for Microrna Detection. *Anal. Chem.* **2016**, *88*, 1294−1302.

(26) Yadavalli, H. C.; Park, S.; Kim, Y.; Nagda, R.; Kim, T.-H.; Han, M. K.; Jung, I. L.; Bhang, Y. J.; Yang, W. H.; Dalgaard, L. T.; Yang, S. W.; Shah, P. Tailed-Hoogsteen Triplex DNA Silver Nanoclusters Emit Red Fluorescence Upon Target miRNA Sensing. *Small* **2024**, *20*, No. 2306793.

(27) Yang, Z.; Hu, L.; Ning, K.; Wu, Y.; Liang, J. A Fluorescence Sensor for Thiram Detection Based on DNA-Templated Silver Nanoclusters without Metal Ion-Mediator. *Food Chem.* **2023**, *413*, No. 135428.

(28) Zhou, B.; Khan, I. M.; Ding, X.; Niazi, S.; Zhang, Y.; Wang, Z. Fluorescent DNA-Silver Nanoclusters in Food Safety Detection: From Synthesis to Application. *Talanta* **2024**, *273*, No. 125834.

(29) Li, R.; Zhu, L.; Yang, M.; Liu, A.; Xu, W.; He, P. Silver Nanocluster-Based Aptasensor for the Label-Free and Enzyme-Free Detection of Ochratoxin A. *Food Chem.* **2024**, *431*, No. 137126.

(30) Yan, C.; Mu, L.; Mei, M.; Wang, Y.; She, G.; Shi, W. Fluorescence Enhancement Method for Aptamer-Templated Silver Nanoclusters and Its Application in the Construction of a β-Amyloid Oligomer Sensor. *Anal. Chem.* **2023**, *95*, 6915−6922.

(31) Rück, V.; Mishra, N. K.; Sørensen, K. K.; Liisberg, M. B.; Sloth, A. B.; Cerretani, C.; M?llerup, C. B.; Kjaer, A.; Lou, C.; Jensen, K. J.; Vosch, T. Bioconjugation of a near-Infrared DNA-Stabilized Silver Nanocluster to Peptides and Human Insulin by Copper-Free Click Chemistry. *J. Am. Chem. Soc.* **2023**, *145*, 16771−16777.

(32) Simmel, F. C.; Yurke, B.; Singh, H. R. Principles and Applications of Nucleic Acid Strand Displacement Reactions. *Chem. Rev.* **2019**, *119*, 6326−6369.

(33) Bi, S.; Yue, S.; Zhang, S. Hybridization Chain Reaction: A Versatile Molecular Tool for Biosensing, Bioimaging, and Biomedicine. *Chem. Soc. Rev.* **2017**, *46*, 4281−4298.

(34) Zhang, S.; Wang, K.; Li, K.-B.; Shi, W.; Jia, W.-P.; Chen, X.; Sun, T.; Han, D.-M. A DNA-Stabilized Silver Nanoclusters/Graphene Oxide-Based Platform for the Sensitive Detection of DNA through Hybridization Chain Reaction. *Biosens. Bioelectron.* **2017**, *91*, 374−379.

(35) Jiang, Y. T.; Guo, Z. Z.; Wang, M. Y.; Cui, J. J.; Miao, P. Construction of Fluorescence Logic Gates Responding to Telomerase and miRNA Based on DNA-Templated Silver Nanoclusters and the Hybridization Chain Reaction. *Nanoscale* **2022**, *14*, 612−616.

(36) Luo, Z.; Li, Y.; Zhang, P.; He, L.; Feng, Y.; Feng, Y.; Qian, C.; Tian, Y.; Duan, Y. Catalytic Hairpin Assembly as Cascade Nucleic

https://doi.org/10.1021/jacsau.4c00291
JACS Au 2024, 4, 2323−2334

Acid Circuits for Fluorescent Biosensor: Design, Evolution and Application. *TrAC, Trends Anal. Chem.* **2022**, *151*, No. 116582.
(37) Kim, H.; Kang, S.; Park, K. S.; Park, H. G. Enzyme-Free and Label-Free miRNA Detection Based on Target-Triggered Catalytic Hairpin Assembly and Fluorescence Enhancement of DNA-Silver Nanoclusters. *Sens. Actuators, B* **2018**, *260*, 140−145.
(38) Yang, M.; Li, H.; Li, X.; Huang, K.; Xu, W.; Zhu, L. Catalytic Hairpin Self-Assembly Regulated Chameleon Silver Nanoclusters for the Ratiometric Detection of CircRNA. *Biosens. Bioelectron.* **2022**, *209*, No. 114258.
(39) Li, Y.; Luo, Z.; Zhang, C.; Sun, R.; Zhou, C.; Sun, C. Entropy Driven Circuit as an Emerging Molecular Tool for Biological Sensing: A Review. *TrAC, Trends Anal. Chem.* **2021**, *134*, No. 116142.
(40) Li, F.; Li, G.; Cao, S.; Liu, B.; Ren, X.; Kang, N.; Qiu, F. Target-Triggered Entropy-Driven Amplification System-Templated Silver Nanoclusters for Multiplexed microRNA Analysis. *Biosens. Bioelectron.* **2021**, *172*, No. 112757.
(41) Lv, H.; Xie, N.; Li, M.; Dong, M.; Sun, C.; Zhang, Q.; Zhao, L.; Li, J.; Zuo, X.; Chen, H.; Wang, F.; Fan, C. DNA-Based Programmable Gate Arrays for General-Purpose DNA Computing. *Nature* **2023**, *622*, 292−300.

https://doi.org/10.1021/jacsau.4c00291
JACS Au 2024, 4, 2323−2334